Minerals Engineering 184 (2022) 107604

Contents lists available at ScienceDirect

Minerals Engineering

journal homepage: www.elsevier.com/locate/mineng

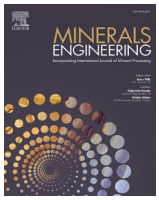

# Effect of mineralogy on Co and Ni extraction from Brazilian limonitic laterites via bioleaching and chemical leaching

Srdjan Stanković [a,*], Mirko Martin [b], Simon Goldmann [a], Hans-Eike Gäbler [a], Kristian Ufer [a], Frank Haubrich [b], Vivian Fernandes Moutinho [c], Ellen Cristine Giese [c], Reiner Neumann [c], José Luciano Stropper [d], Jens Stummeyer [a], Stephan Kaufhold [a], Reiner Dohrmann [a,e], Anne Oxley [f,g], Herwig Marbler [a], Axel Schippers [a,*]

[a] Bundesanstalt für Geowissenschaften und Rohstoffe, Stilleweg 2, 30655 Hannover, Germany
[b] G.E.O.S. Ingenieurgesellschaft mbH, Schwarze Kiefern 2, 09633 Halsbrücke, Germany
[c] Centro de Tecnologia Mineral, Avenida Pedro Calmon, 900, 21941-908 Rio de Janeiro, Brazil
[d] Companhia de Pesquisa de Recursos Minerais, Rua Banco de Província 105, Santa Tereza, 90840-030 Porto Alegre, Brazil
[e] Landesamt für Bergbau, Energie und Geologie, Stilleweg 2, 30655 Hannover, Germany
[f] Brazilian Nickel PLC, 10 Lonsdale Gardens, Tunbridge Wells TN1 1NU, UK
[g] Scientific Associate of the Natural History Museum, London, UK

ARTICLE INFO

*Keywords:*
Reductive bioleaching
Laterites
Mineralogy
*Acidithiobacillus*
Nickel
Cobalt

ABSTRACT

Iron-rich, limonitic laterites may contain economic grades of nickel and cobalt, but efficient extraction of these metals from such ores is still a challenge. In this study, four samples of limonitic laterites originating from the Barro Alto mine in Brazil were subjected to detailed quantitative mineralogical examination followed by bioleaching and chemical leaching tests including mineralogical leaching residue analyses. Bioleaching experiments with pure cultures and addition of elemental sulfur were conducted in 2L bioreactors under aerobic conditions with the sulfur-oxidizing acidophilic bacteria *Acidithiobacillus (At.) thiooxidans* and *At. caldus*, and under anaerobic conditions with *At. ferrooxidans*. Aerobic bioleaching of laterites with *At. thiooxidans* and *At. caldus* allowed for a lower pH of 1.0 and 1.1 respectively, and thus a higher Ni and Co extraction than anaerobic bioleaching with *At. ferrooxidans* at pH 1.5. Extraction of cobalt via bioleaching was in the range of 68–88 %, while extraction of nickel was between 17 % and 56 %. Mineralogical and geochemical analysis (XRD, SEM-MLA, DSC, LA-ICP-TOFMS, XRF) was conducted to (i) identify mineral phases, which are attacked by bioleaching and (ii) estimate the portions of Co and Ni, which are released by bioleaching of different mineral phases. Cobalt was mostly hosted by Mn-rich mineral phases, which were dissolved after reduction with ferrous iron generated by bacterial metabolism during oxidation of sulfur. Nickel was mostly hosted by goethite, the most abundant mineral phase, but nickel was also present in Mn-rich minerals (e.g. asbolane) and magnesium silicates (e.g. serpentine). Mineralogical and geochemical data revealed that goethite was almost unleached in all samples and nickel was mostly released from Mn-rich mineral phases and magnesium silicates. Results of this research were able to confirm reductive bioleaching of Mn-rich phases. Chemical leaching tests performed with different concentrations of sulfuric acid and with hydrochloric acid, and with sulfuric acid plus ferrous iron as a reducing agent supported bioleaching results. The results are not supporting published data on substantial reductive dissolution of goethite via ferric iron reduction activity of acidophilic bacteria.

## 1. Introduction

Processing of iron-rich, limonitic laterites in order to produce nickel and cobalt is a challenge due to the complex and heterogeneous mineralogy of these laterites, which are mainly consisting of refractory iron oxide minerals such as goethite and hematite (Brand et al., 1998). Pyrometallurgical treatment is not applicable to limonitic laterites, consequently some mining companies remove the limonitic horizon,

* Corresponding authors.
*E-mail addresses:* srdjan.stankovic@bgr.de (S. Stanković), axel.schippers@bgr.de (A. Schippers).

https://doi.org/10.1016/j.mineng.2022.107604
Received 30 March 2022; Accepted 28 April 2022
Available online 20 May 2022

which is close to the Earth́s surface, just in order to get to the deeper saprolitic ores constituted mostly of silicate minerals. Substantial amounts of nickel and cobalt are locked in large stockpiles of iron-rich laterites, waiting for a suitable processing technology. Conventional hydrometallurgical options for processing limonitic laterites include the CARON process, atmospheric tank leaching, high pressure acid leaching and heap leaching (McDonald and Whittington, 2008; Stanković et al., 2020).

A relatively new and promising approach to unlock potential of limonitic laterites is the biohydrometallurgical processing of the laterites by application of the reductive bioleaching technology (du Plessis et al., 2011). Laterite bioleaching is based on the ability of certain species of acidophilic, chemolithoautotrophic bacteria, e.g. belonging to the genus *Acidithiobacillus (At.),* to reduce ferric iron during metabolic oxidation of elemental sulfur to sulfuric acid under anaerobic and aerobic conditions (Hallberg et al., 2011; Johnson et al., 2013; Johnson and du Plessis, 2015; Marrero et al., 2015; 2017; 2020; Smith et al., 2017; Santos et al., 2020; Santos and Schippers, 2022; Malik and Hedrich, 2022). Bridge and Johnson (2000) showed that the organoheterotrophic acidophilic bacterium *Acidiphillium* SJH has the ability to promote dissolution of iron oxide minerals during anaerobic respiration on ferric iron. This led to the idea of using acidophilic bacteria with the ability to reduce iron for leaching of nickel and cobalt from the goethite-rich limonitic ores (Hallberg at al., 2011; du Plessis et al., 2011). In this type of ores, nickel, and to a lower extent cobalt atoms substitute atoms of iron in the crystal lattice of the goethite which is the dominant mineral phase in limonitic laterites, but Ni and Co also occur in different other mineral phases, e.g. Mn oxides (Watling et al., 2011). Efficient extraction of nickel mostly depends on dissolution of goethite, while most of the cobalt is usually hosted by asbolane-lithiophorite minerals (Brand et al., 1998). The potential advantages of the bioleaching approach over established ore processing technologies are lower energy consumption (the temperature during bioleaching is in the range of 30–45 °C), lower acid consumption (bacteria generate sulfuric acid during metabolic sulfur oxidation) and less expensive equipment due to relatively moderate acidic conditions (the pH value of the leach solution is in the range of 0.8–1.7). This technology should provide leaching of nickel and cobalt from limonitic ores with lower capital and operational expenses in comparison to competing technologies (du Plessis et al., 2011; Johnson and du Plessis, 2015).

In this study, leaching of nickel and cobalt from limonitic laterites originating from the Barro Alto mine in Brazil was investigated. The main goal of this research was to compare chemical leaching of the laterites (with and without addition of the reducing agents) with bioleaching using pure cultures of the acidophilic bacteria *At. ferrooxidans*, *At. thiooxidans* and *At. caldus* under anaerobic (*At. ferrooxidans)* and aerobic conditions (*At. thiooxidans* and *At. caldus*). Another goal was to investigate if anaerobic or aerobic bioleaching of limonitic laterites is more efficient, thus pure culture bioleaching experiments were carried out while most published studies used mixed cultures. In addition, a comprehensive quantitative mineralogical examination of the samples before and after leaching experiments was conducted in order to understand the bioleaching process.

## 2. Materials and methods

### 2.1. Laterite samples

Lateritic material was collected in the Anglo American-owned Barro Alto mine located in the state of Goiás, Central Brazil. Overall, four samples were taken with these acronyms: BaC, 1P5, BaSt and LimSt. Samples designated as BaC and 1P5 were collected from the limonitic horizon within the open pit: 1P5 was taken as a fresh excavated sample (around 25 kg) to access the saprolitic material below. BaC was taken as a bulk sample from seven different channels (213 kg in total) at three different locations in the opencast mine, in order to obtain representative fresh limonitic sample material. It was a yellowish-reddish to brownish-colored, fine-grained clayey-silty material, totally decomposed and disaggregated. The samples BaSt and LimSt were obtained from two different stockpiles. LimSt was taken from the surface to about 0.5 m depth of a stockpile (approx. 30 kg) and BaSt was drilled as a 16 m deep borehole within one of the large stockpiles in the mine with a total sample weight of 181 kg. These stockpile samples were ochercolored, fine-grained clayey-silty materials, completely decomposed and disaggregated. Images of the sampling sites are shown in the supplementary material (Fig. S1).

The batches of each individual sample were mixed and thoroughly homogenized in roller drums. The samples were split using a lab-scale ripple divider into four batches each. Samples were then sieved to size $< 2$ mm and used for analyses and laboratory experiments.

### 2.2. Physical properties, mineralogical and chemical analyses of solid samples

Comprehensive quantitative chemical and mineralogical analyses of the laterite samples before and after leaching experiments were performed.

#### 2.2.1. Grain size distribution and specific surface area

The grain size distribution was determined via X-ray granulometry (Sedigraph, Micromeritics) following a specific sample pre-treatment based on a physical disaggregation (ultrasound) and addition of a dispersing agent (Müller et al., 2009). Because of the high iron oxide content, the specific density was determined using helium pycnometry (AccuPyc 1330, Micromeritics). The sample volume was calculated from the observed pressure change that helium undergoes when it expands from one chamber containing the sample into another chamber without sample. Density parameters were used for analysis of grain size distribution.

The specific surface area was determined by $N_2$ adsorption with a Micromeritics Gemini III 2375 surface area analyzer (Kaufhold et al., 2010).

#### 2.2.2. Total chemical composition

The mass fraction of metals and other elements in solid samples was determined via wavelength-dispersive X-ray fluorescence (XRF, PANalytical Zetium WD-Spectrometer). Samples were air-dried, crushed, homogenized, split and 2 g each ground with zirconium oxide grinding media in a McCrone mill under ethanol for 12 min. The ground material was dried, homogenized and prepared into powder cuvettes.

Selected samples were also analyzed by peroxide fusion ICP-MS (FUSMS-$Na_2O_2$, Actlabs).

Total sulfur and organic carbon contents were analyzed using a LECO CS 230 carbon–sulfur analyzer.

#### 2.2.3. X-ray diffraction (XRD) with Rietveld refinement

XRD patterns were recorded using a PANalytical X'Pert PRO MPD Θ-Θ diffractometer (Co-Kα radiation generated at 40 kV and 40 mA), equipped with a variable divergence slit (20 mm irradiated length), primary and secondary soller, diffracted beam monochromator, point detector, and a sample changer (sample diameter 28 mm). The samples were investigated from 1° to 80° 2Θ with a step size of 0.03° 2Θ and a measuring time of 3 sec per step. The back loading technique was used for specimen preparation.

Rietveld refinement of the experimental XRD data was conducted using the software Profex/BGMN (Döbelin & Kleeberg, 2015; Bergmann et al., 1998). The mineral phases were identified during the Rietveld refinement process.

#### 2.2.4. Scanning electron microscopy (SEM) with Mineral Liberation Analysis (MLA) software

Automated mineralogical analysis was performed with the FEI

Quanta MLA 650F (ThermoFischer Scientific, USA) scanning electron microscope equipped with two energy-dispersive X-ray (EDX) detectors (XFlash 5030 Silicon Drift Detector; Bruker Nano, USA) and Mineral Liberation Analysis (MLA) software (Fandrich et al., 2007). Carbon coated polished sections of the four laterite samples and selected bioleaching residues were prepared. The MLA software uses the EDX system of the SEM combined with backscattered electron (BSE) imaging for automatic identification of mineral phases. Mineral particles are identified by their specific grey value in the BSE image after removal of background. Within identified particles, EDX measurements are performed and the characteristic X-ray spectrum of each analysis spot is compared with the X-ray spectra of defined phases stored in a database. The characteristic X-ray peaks in the spectrum are related to the respective elements present in the particles. Therefore, phases are identified by their chemical composition and neither crystallographic nor structural information is taken into account. After classification, the identified phases are displayed on a MLA image and the relative abundances of the mineral phases (modal mineralogy) are given.

#### 2.2.5. Differential scanning calorimetry (DSC)

Thermoanalytical investigations were performed using a Netzsch 449 F3 Jupiter (Netzsch, Germany) thermobalance equipped with a DSC/TG (thermogravimetry) sample holder linked to a Netzsch QMS 403C Aeolus mass spectrometer (MS). 100 mg of powdered material previously equilibrated at 53 % relative humidity (RH) was heated from 25 −1150 °C with a heating rate of 10 K/min. DSC curves representing exothermal and endothermal reactions induced by heating were recorded as well as gravimetrical curves showing the mass losses of the samples as a function of temperature. Hydroxides as goethite and gibbsite dehydroxylate between 250 and 350 °C and hence at much lower temperatures compared with clay minerals. The determination of the mass loss of the samples between 250 and 350 °C, therefore, could be used to estimate the goethite (+gibbsite) content based on the assumption that goethite loses about 10.1 mass% water in this T-range. Natural organic material (NOM), however, oxidizes and decomposes in the same T-range and hence could affect the values. In order to characterize NOM, evolved gases, particularly $CO_2$ and $H_2O$, were simultaneously analyzed by mass spectroscopy (STA, simultaneous thermal analysis).

#### 2.2.6. Laser ablation-inductively coupled plasma-time of flight mass spectrometry (LA-ICP-TOFMS)

Quantified element distribution maps were obtained from polished sample sections (previously analysed by SEM-MLA) using a laser ablation-inductively coupled plasma-time of flight mass spectrometry system (LA-ICP-TOFMS). The LA-ICP-TOFMS system consists of the 193 nm laser ablation system IRIDIA (Teledyne CETAC Technologies, Omaha, USA) equipped with a fast washout Cobalt Sample Cell and an Aerosol Rapid Introduction System (ARIS) coupled to the icpTOF 2R inductively coupled plasma-time of flight mass spectrometer (TOFWERK AG, Thun, Switzerland). The software Chromium 2.7 (Teledyne CETAC Technologies, Omaha, USA) controlled the laser. The software TOFpilot (TOFWERK AG, Thun, Switzerland) operated the mass spectrometer. The software HDIP (Teledyne CETAC Technologies, Omaha, USA) was used for data evaluation. Helium was used as the transport gas. A square 10 μm spot was used for ablation of sample material at a fluence of 7.22 J/cm$^2$ with a repetition rate of 80 Hz and a dosage of 1 pulse/spot resulting in a scan speed of 800 μm/s. In this way areas of about 5 mm * 15 mm were gapless ablated for a single map. Ten gas blanks and 10 lines on a calibration material (CM) were recorded at equally distributed time intervals together with the sample. The CM was prepared from an aliquot of the solid residue of a bioleaching experiment. The CM was wet ground in a planetary ball mill (Planetary Micro Mill PULVERISETTE 7 premium line, Fritsch, Idar-Oberstein, Germany) using 3 mm agate balls and an agate grinding bowl. After grinding and freeze drying the CM was characterized by XRF and a sulfur analyser (LECO CS 230) and pressed to a pellet for use in LA-ICP-TOFMS.

Raw data of the TOF instrument were imported into the HDIP software for further processing. After background correction based on the recorded gas blanks, element distribution maps in counts per seconds (cps) were calculated. Calibration functions were calculated based on the records of the CM and applied on the sample data to obtain concentration-related element distribution maps. A distribution map of the sum of the concentrations of Mg, Al, Si, Cr, Mn, and Fe was calculated. Based on this map, areas consisting of sample material and resin could be discerned. Sum normalisation of the previously external calibrated concentrations was applied only on areas consisting of sample material to account for different ablation yields of sample and CM. In the sum normalisation step the sum of $Na_2O$, MgO, $Al_2O_3$, $SiO_2$, S, $Cr_2O_3$, MnO, $Fe_2O_3$, CoO, and NiO was normalized to 100%. Element distribution maps of the normalised data were used for the calculations of mean concentrations and portions of volumes of interest (VOI).

The accuracy of the LA-ICP-TOFMS data was evaluated by comparison with XRF bulk data of the four laterite deposit samples. LA-ICP-TOFMS bulk concentrations were obtained from the mean values of the mapped areas on the polished sections consisting of sample material. Concentrations of MgO, $Al_2O_3$, $SiO_2$, MnO, $Fe_2O_3$, Co, and Ni were compared by calculating the absolute value of the difference between both methods divided by the XRF concentration. The median value of all relative deviations was 12% ($25^{th}$ percentile = 5%, $75^{th}$ percentile = 27%, n = 28).

### 2.3. Liquid sample analyses

Liquid samples were obtained in leaching experiments. Concentrations of dissolved metals were determined by ICP-OES. Ferrous iron concentrations in solution were measured by a colorimetric assay using ferrozine (Lovely and Philips, 1987). Total iron was quantified by adding an excess of ascorbic acid to reduce soluble ferric iron to ferrous iron. Ferric iron was determined from the difference between the total and ferrous iron concentrations. The pH was measured with electrodes and the redox potential was measured with platinum-silver/silver chloride electrodes. Numbers of bacteria in liquid samples were determined after staining bacteria with SYBR Green and counting them under fluorescence microscope (Hedrich et al., 2016).

### 2.4. Chemical leaching experiments

Chemical leaching experiments were conducted with 5 % and 30 % sulfuric acid, 5 % sulfuric acid with addition of 7 g/L ferrous iron at 20 °C and with 20 % hydrochloric acid at 60 °C. The solid to liquid ratio was 1:5 (20 % pulp density). Duration of the leaching experiments with 5 % sulfuric acid, 5 % sulfuric acid with addition of 7 g/L ferrous iron and 20 % hydrochloric acid was 24 h. Duration of experiment with 30 % sulfuric acid as lixiviant was 168 h. The leaching experiments were performed in a 1 L beaker, which contained 500 mL of solution, stirring speed was 300 rpm using a Cat R 18 stirrer (Zipperer GmbH, Ballrechten-Dottingen, Germany).

### 2.5. Bioleaching experiments

Reductive bioleaching experiments were conducted in 2 L bioreactors Fermac 310/60 (Electrolab, Tawkesbury, UK), with a working volume of ca. 1.5 L and constant pH and temperature. Bioreactors were inoculated with pure cultures of the type strains of three acidophilic bacteria: the mesophilic sulfur-oxidizer *At. thiooxidans,* the mesophilic iron- and sulfur-oxidizer *At. ferrooxidans* and the moderately thermophilic sulfur-oxidizer *At. caldus*. Before inoculation, the bacteria were cultivated in 300 mL shake flasks containing 150 mL of bacterial culture in basal salt solution at pH 3 composed as described by Wakeman et al. (2008), and supplemented with 1 % (w/v) of elemental sulfur. Flasks were placed on an orbital shaker at speed of 120 rpm for 7 days at

constant temperature of 30 °C or 45 °C in case of *At. caldus*. Bioreactors containing 1350 mL of basal salts solution at pH 2.5 and 1 % (w/v) of sulfur were inoculated with 150 mL of active bacterial cultures containing approximately $10^8$ cells/mL. In order to produce enough bacterial biomass, bioreactors were run for three days prior to addition of the laterite samples. Each bioreactor was supplied with 75 g of laterite sample (5 % pulp density). Bioreactors inoculated with *At. thiooxidans* were maintained at temperature of 30 °C and the pH of the suspension was kept at 1.0 by automatic addition of either 2 M sulfuric acid or 2 M sodium hydroxide controlled via permanent pH electrode measurements using the Fermac 360 controller. Air supply was constant at a rate of 1.5 L/min. Bioreactors inoculated with *At. ferrooxidans* were maintained at 30 °C, pH 1.5. After addition of the sample, air supply was turned off and switched to dinitrogen gas. In order to maintain anaerobic conditions, bioreactors were flushed with dinitrogen gas daily for one hour at a rate of 800 mL/min and twice per week 50 mL of $CO_2$ were added. Bioreactors inoculated with *At. caldus* were maintained at 45 °C, pH 1.1, with constant supply of air at a rate of 1.5 L/min. Not inoculated control bioreactors contained basal salts solution, 1 % (w/v) of sulfur and 75 g of the sample. Temperatures in control bioreactors were maintained at either 30 or 45 °C at a constant pH 1.2. To the control bioreactors, formic acid was added to a final concentration of 0.5 mM to inhibit acidophilic bacteria as potential contaminants (Zhang et al., 2020). Acid and base consumptions were recorded until the end of each experiment. All experiments were conducted in duplicate, except controls. Duration of experiments was 21 days. Overall, 24 inoculated bioreactor experiments and 8 control reactors were run. Liquid samples were regularly taken and analyzed and solid residues from selected bioleaching experiments were analyzed to verify which minerals had been dissolved.

## 3. Results and discussion

### 3.1. Chemical composition and physical properties of the ore samples

Results of the chemical analysis of the four laterite samples are presented in Table 1. The chemical composition was typical for limonitic laterites, with a high content of $Fe_2O_3$. A more detailed chemical analysis can be found in the Supplementary material, Table S1.

Particle size distribution of the samples is shown in Supplementary material Fig. S2. The dominant grain size fraction in all samples was smaller than 0.002 mm, followed by medium silt and fine/coarse silt fractions. Sand fractions are present in minor amounts. Specific densities (3.23–3.97 g/cm$^3$) correlated very well with the $Fe_2O_3$ content. BaSt, BaC and LimSt had surface areas of 67, 64 and 61 m$^2$/g, respectively, while 1P5 had a much lower surface area of 34 m$^2$/g.

### 3.2. Chemical leaching experiments

Fig. 1 shows results of nickel and cobalt extraction after chemical leaching with sulfuric acid and hydrochloric acid. Leaching with 5 % sulfuric acid resulted in very low extraction of Ni from 1P5, BaC and LimSt samples (0.01 %, 2% and 0.02 %, respectively), but nickel leaching from BaSt sample was substantially higher (16 %). Addition of 7 g/L ferrous iron in 5 % sulfuric acid had a beneficial effect on Ni extraction: the leaching degree of nickel from BaSt, BaC and LimSt samples increased to 26.1 %, 13.6 % and 15.5 % respectively, while leaching degree of Ni from 1P5 sample was negligible (Fig. 1). The dissolution rate of Fe(III) oxides is a function of their surface area (Schwertmann, 1991), the lowest surface area of the 1P5 sample in comparison to the other samples is likely one of the reasons for the low dissolution rate of iron oxides in this sample. Increase in nickel extraction after addition of ferrous iron is a consequence of the reductive dissolution of other mineral phases, which contained a significant amount of Ni and Co (discussed below). Application of reducing agents, such as ferrous iron, iron powder, $SO_2$, $S_2O_3^{2-}$ and $Na_2SO_3$ increases leaching of cobalt and nickel from lateritic ores (Senanayake et al. 2011, Li et al. 2011, Luo et al., 2015, Komnitsas et al., 2019). Senanayake et al. (2011) reported increased nickel extraction from synthetic Ni-containing goethite and lateritic ore after addition of 12 g/L ferrous sulfate. MacDonald and Whittington (2008) suggest that protonation of iron oxide minerals might be facilitated in presence of ferrous iron. Mechanisms of interactions between ferrous iron and goethite are complex and not completely explained (Handler et al., 2009).

Addition of ferrous iron significantly improved cobalt extraction in all samples: leaching efficiency of cobalt from BaSt, BaC, Lim St and 1P5 samples increased to 75 %, 67 %, 77 % and 3 %, respectively. Cobalt is associated with Mn-phases (such as asbolane, see below) that are rapidly dissolved by reduction with ferrous iron. Coefficient of correlation between Mn and Co extractions for all samples was $r^2 = 0.9$, confirming that cobalt was mostly located in the manganese mineral phases, while the coefficient of correlation for Mn and Ni extractions was $r^2 = 0.42$, which indicates that certain amount of nickel was leached from Mn-rich mineral phases (supplementary material Fig. S3).

Leaching with 20 % hydrochloric acid for 24 h at a temperature of 60 °C resulted in a higher nickel and cobalt extraction in comparison to experiments with sulfuric acid (Fig. 1) likely due to facilitated protonation of iron oxide minerals by hydrochloric acid and the formation of $Cl^-$-complexes of transition metals (Senanayake et al., 2011).

### 3.3. Bioleaching experiments

Changes in concentrations of nickel, cobalt, ferrous and total iron, redox potential, and the number of bacteria over time during bioleaching experiments are presented in supplementary material (Figures S4 to S11). Fig. 2 shows values for ferrous iron and Fig. 3 shows nickel and cobalt extraction values at the end of the experiments after 21 days of bioleaching. During the bioleaching experiments the acidophilic bacteria that used sulfur as an energy source reduced ferric iron dissolved by sulfuric acid from lateritic material. In the bioreactors, the redox potential almost exclusively depended on the ferric to ferrous iron ratio. Reduction of ferric iron to ferrous iron leads to a decrease in the redox potential of the solution in agreement with literature data (Marrero et al., 2015; Santos et al., 2020).

#### 3.3.1. Bioleaching of different samples in comparison to chemical controls

Leaching of nickel was more efficient in inoculated bioreactors in comparison to controls. In inoculated bioreactors the redox potential decreased, while in non-inoculated bioreactors there was no significant change in redox potential. Leaching of Co was much more efficient in inoculated bioreactors and leaching degrees for cobalt were relatively high. Even in C bioreactors (see 3.3.2), which contained the lowest concentrations of reduced iron, cobalt extractions were similar to values obtained in T and F bioreactors (see 3.3.2). This result indicates that even relatively low concentrations of ferrous iron were sufficient for

**Table 1**
Results of the XRF analysis of the laterite samples given in wt% or mg/kg.

| | $SiO_2$, % | $Al_2O_3$, % | MgO, % | $Fe_2O_3$, % | MnO, % | Cr, mg/kg | Co, mg/kg | Ni, mg/kg |
|---|---|---|---|---|---|---|---|---|
| BaSt | 26.20 | 4.75 | 9.41 | 42.39 | 0.82 | 15,760 | 1266 | 13,610 |
| BaC | 9.42 | 7.63 | 2.10 | 61.44 | 0.92 | 21,760 | 1192 | 13,100 |
| LimSt | 14.25 | 4.33 | 3.15 | 58.72 | 1.47 | 26,070 | 2651 | 14,490 |
| 1P5 | 3.02 | 3.41 | 1.20 | 74.95 | 0.21 | 25,100 | 243 | 9524 |

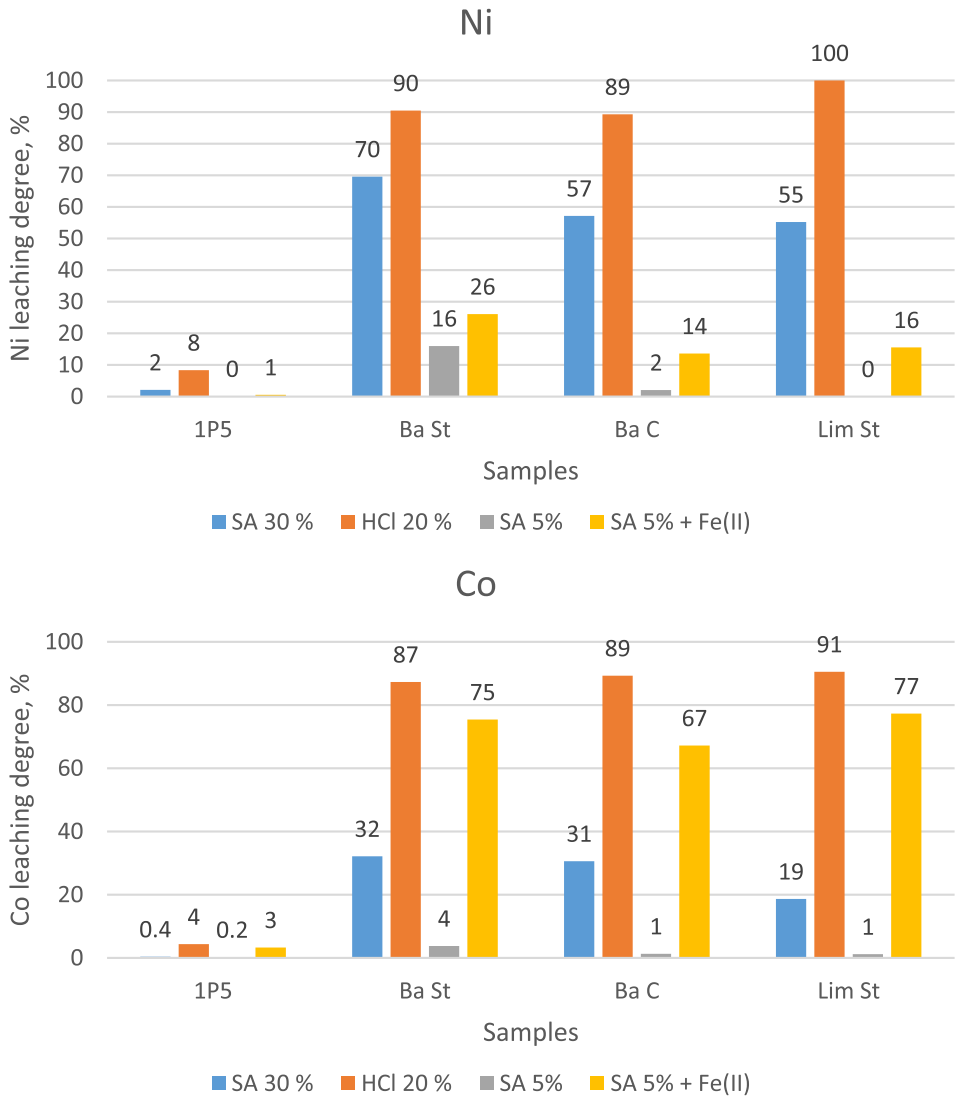


**Fig. 1.** Percentages of extracted Ni (top) and Co (bottom) in chemical leaching experiments. SA 30 %: leaching with 30 % sulfuric acid, 168 h at 20 °C; HCl 20 %: leaching with 20 % hydrochloric acid, 24 h, 60 °C; SA 5 %: leaching with 5% sulfuric acid, 24 h, 20 °C: SA 5 % + Fe(II): leaching with 5% sulfuric acid and 7 g/L ferrous iron, 24 h, 20 °C.

effective leaching of cobalt, probably because bacteria can "recycle" ferrous iron that was oxidized in reaction with Mn-rich mineral phases such as asbolane. The percentage of Ni leached from BaSt sample (Fig. 3) was substantially higher in comparison to the other three samples, both, in inoculated and non-inoculated bioreactors, likely since this sample contained a high amount of Ni in serpentine being dissolved during bioleaching as discussed below.

### 3.3.2. *Bioleaching by different Acidithiobacillus species*

Looking at the percentage of reduced iron relative to total iron in the solution at the end of experiments (Fig. 3), it can be concluded that the most efficient ferric iron-reducer was *At. ferrooxidans* (F bioreactors) under anaerobic conditions at constant pH 1.5, followed by *At. thiooxidans* (T bioreactors) at pH 1.0, while *At. caldus* (C bioreactors) at pH 1.1 was a relatively inefficient ferric iron-reducer. Concentrations of ferrous iron at the end of experiments were highest in bioreactors inoculated with *At. thiooxidans* and concentrations of total dissolved iron were highest in bioreactors inoculated with *At. thiooxidans* and *At. caldus*. These two sulfur-oxidizing species can survive in the environment at very low pH. According to literature data, *At. thiooxidans* can survive in solutions with pH as low as 0.5, while the lower limit of pH for *At. caldus* is around pH 1 (Schippers, 2007). *At. ferrooxidans* is less tolerant to extremely acidic conditions, with lower limit of pH 1.3, therefore the pH in F bioreactors inoculated with these bacteria was maintained at pH of 1.5. Dissolution of iron from lateritic ores was depending on the concentration of sulfuric acid in the solution, thus more iron was dissolved in T and C bioreactors than in F bioreactors. Similar results were reported by Marrero et al. (2017). As a result, on average more ferric iron was reduced in T bioreactors than in F bioreactors. Since *At. caldus* was a relatively inefficient ferric iron-reducer, the lowest concentrations of ferrous iron were detected in C bioreactors.

### 3.3.3. *Acid and base consumption for pH maintenance in bioreactor experiments*

Consumption of $H_2SO_4$ and NaOH for keeping the pH constant during the bioleaching experiments is presented in Fig. 4. Consumption of NaOH in T and C bioreactors was substantial, and no consumption of $H_2SO_4$ was recorded in these bioreactors, except for a relatively small amount consumed during bioleaching of the 1P5 sample. Bioreactors F consumed much lower amounts of base in comparison to T and C bioreactors and a certain amount of sulfuric acid. *At. ferrooxidans* preferentially uses ferrous iron as an energy source, but in absence of iron, these bacteria can switch to sulfur metabolism. *At. thiooxidans* and *At. caldus* are obligatory sulfur-oxidizers, so these bacteria are efficient in

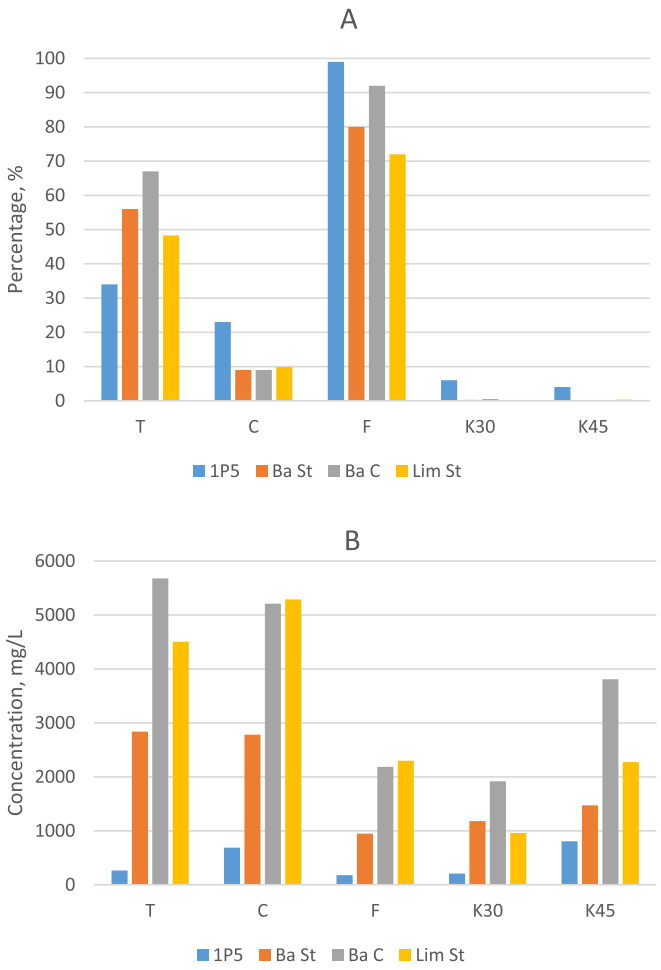


**Fig. 2.** Ferrous iron as a percentage of the total iron (A) and total iron concentrations (B) at the end of bioleaching experiments. T: bioreactors inoculated with *At. thiooxidans;* C: bioreactors inoculated with *At. caldus;* F: bioreactors inoculated with *At. ferrooxidans;* K30 and K45: non-inoculated controls at 30 °C and 45 °C.

oxidation of sulfur. That explains a relatively high base consumption in T and C bioreactors, the rate of acid production was higher than acid consumption, thus a substantial amount of NaOH was consumed in order to maintain the desired pH value.

### 3.3.4. *Comparison of Ni and Co extraction efficiency in bioleaching and chemical leaching experiments*

Values given in Table 2 provide a comparison of Ni and Co extraction efficiency in bioleaching and chemical leaching experiments. The highest mean leaching degree of nickel was achieved with 20 % hydrochloric acid after 24 h at 60 °C (93 %) followed by 30 % sulfuric acid after 168 h at 20 °C (60 %). The average leaching degrees obtained after bioleaching were significantly lower, with approximately 32 % and 35 % of extracted Ni in T and F bioreactors, respectively, and 24 % in F bioreactors. This difference of bioleaching vs. chemical leaching could likely be explained by the much higher acid concentration in chemical experiments allowing also for a dissolution of Ni-bearing Fe-oxides/hydroxides such as goethite to a different degree for the four samples as discussed below. However, a higher acid concentration means higher processing costs as an argument for bioleaching despite a lower Ni extraction efficiency. Lower amounts of leached nickel in F bioreactors can be explained by a higher pH in comparison to T and C bioreactors. Addition of ferrous iron in the chemical leaching experiments had a visible but limited effect on an increase of nickel leaching. Dissolution of iron oxide and hydroxide minerals (mostly goethite) is required in order to achieve satisfactory leaching of nickel, particularly in BaC and LimSt samples. For effective dissolution of goethite, it is obviously mandatory to apply high concentrations of acid, such as 30 % sulfuric acid or 20 % hydrochloric acid. Highest mean leaching degree of cobalt was achieved after leaching with 20 % hydrochloric acid (89 %). Results of bioleaching were also very good, T and C bioreactors reached approximately 83 % and 84 % respectively, and F bioreactors 74 % of cobalt extraction (mean values). Average leaching degrees of cobalt with 5 % and 30 % sulfuric acid were low (2 % and 27 %, respectively), which confirms the critical role of ferrous iron as a reducing agent for Mn-phases in extraction of cobalt from laterites as discussed below.

## 3.4. *Mineralogy and geochemistry*

Cobalt and nickel were released by bioleaching experiments. Mineralogical and geochemical characterization of the original and bioleached samples was done to identify which phases either are attacked by bioleaching or remain more or less untouched by this process. Besides this, it is of interest to know in which phases Co and Ni remain after bioleaching. This knowledge could be used to improve bioleaching. A description of strengths and weaknesses of the particular analytical methods for quantitative mineralogical analyses is provided in the supplementary material (Table S3).

Mineral phases that were dissolved during bioleaching could be identified by comparing mineralogical data of the original sample and

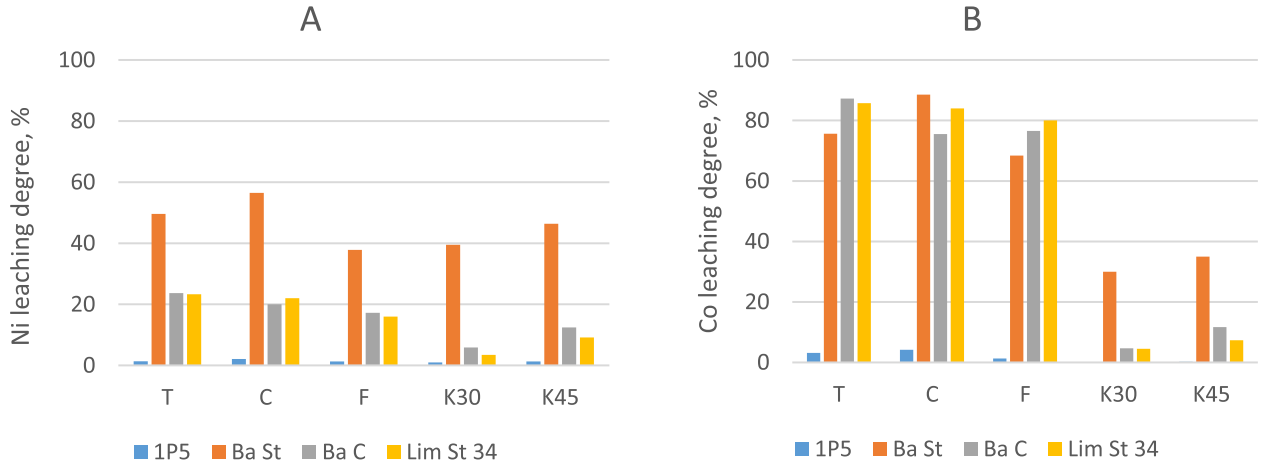


**Fig. 3.** Percentage of extracted Ni (A) and Co (B) at the end of bioleaching and chemical control experiments. T: bioreactors inoculated with *At. thiooxidans;* C: bioreactors inoculated with *At. caldus;* F: bioreactors inoculated with *At. ferrooxidans;* K30 and K45: non-inoculated controls at 30 °C and 45 °C.

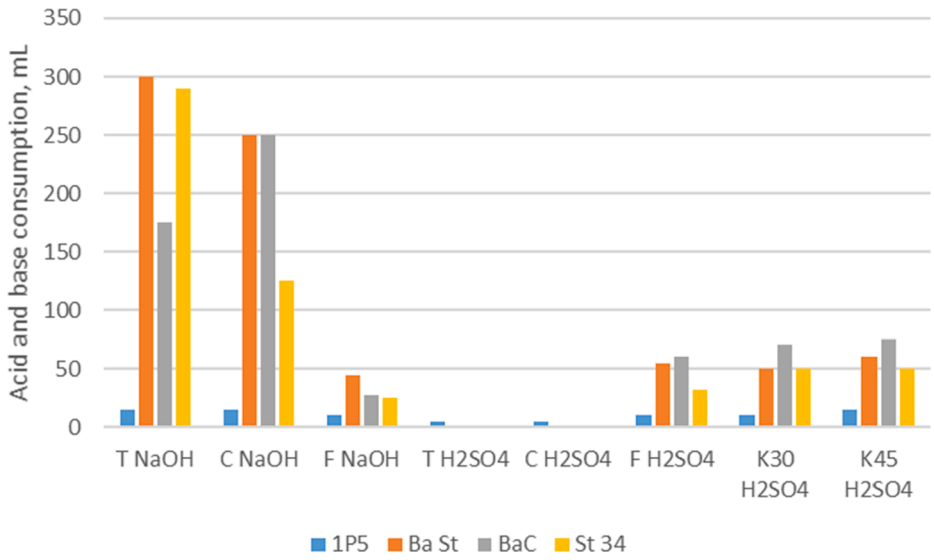


**Fig. 4.** Consumption of 2 M NaOH and 2 M $H_2SO_4$ during bioleaching experiments. T: bioreactors inoculated with *At. thiooxidans;* C: bioreactors inoculated with *At. caldus;* F: bioreactors inoculated with *At. ferrooxidans;* K30 and K45: non-inoculated controls at 30 °C and 45 °C.

**Table 2**
Final leaching degrees of nickel (top) and cobalt (bottom) in percent after chemical leaching and bioleaching experiments. SA 30 %: leaching with 30 % sulfuric acid, 168 h at 20 °C; HCl 20 %: leaching with 20 % hydrochloric acid, 24 h, 60 °C; SA 5 %: leaching with 5% sulfuric acid, 24 h, 20 °C; SA 5 % + Fe(II), leaching with 5% sulfuric acid and 7 g/L ferrous iron, 24 h, 20 °C; C: bioreactors inoculated with *At. caldus*; F: bioreactors inoculated with *At. ferrooxidans*; T: bioreactors inoculated with *At. thiooxidans*; K30 and K45: non-inoculated controls at 30 °C and 45 °C.

| Ni leaching degree | SA 30%, % | HCl 20%, % | SA 5%, % | SA 5% + Fe(II), % | T, % | C, % | F, % |
|---|---|---|---|---|---|---|---|
| Ba St | 69 | 90 | 16 | 26 | 50 | 56 | 38 |
| Ba C | 57 | 89 | 2 | 14 | 24 | 20 | 17 |
| Lim St | 55 | 100 | 0.02 | 15 | 23 | 30 | 18 |
| 1P5 | 2 | 8 | 0.1 | 0.6 | 1 | 2 | 1 |
| Mean (without 1P5) | 60 | 93 | 6 | 18 | 32 | 35 | 24 |
| **Co leaching degree** | **SA 30%, %** | **HCl 20%, %** | **SA 5%, %** | **SA 5% + Fe(II), %** | **T, %** | **C, %** | **F, %** |
| Ba St | 32 | 87 | 4 | 75 | 76 | 88 | 68 |
| Ba C | 30 | 89 | 1 | 67 | 87 | 75 | 76 |
| Lim St | 19 | 90 | 1 | 77 | 86 | 87 | *75* |
| 1P5 | 0.4 | 4 | 0.2 | 3 | 3 | 4 | 1 |
| Mean (without 1P5) | 27 | 89 | 2 | 73 | 83 | 84 | 74 |

its solid residue obtained after bioleaching. The portions of the dissolved phases could be assessed as well. In order to estimate how much Co or Ni was leached from which phase, the Co and Ni contents of the different phases must also be known. These phase-specific Co and Ni contents could be estimated based on the LA-ICP-TOFMS data (TOF data) as discussed below.

### 3.4.1. Comparison of mineralogical composition obtained by SEM-MLA and XRD

The mineralogical composition of the four laterite samples as well as of selected bioleached residues of the experiments with *At. thiooxidans* (T1) was determined. Mineral phases (in a broader sense) were identified and quantified by SEM-MLA and XRD and the data are compiled in Table 3. XRD plots and SEM-MLA images and data are shown in several figures (S12-S19) of supplementary material. Visualization of particular mineral grains with their elemental composition is shown in Figs. S20-S23. Since SEM-MLA and XRD use different fundamental approaches, their results are compared and discussed together.

XRD identified the iron oxide/hydroxide phases goethite and hematite with goethite being the most important phase with mass fractions between 54 % and 94 % in the original samples BaSt, BaC, LimSt, and 1P5. Magnetite detected via XRD is included as spinel in Table 3. By SEM-MLA, these phases were identified and included as iron oxide/hydroxides, which are principally characterized by iron and oxygen without any other element of significance, and this includes goethite and hematite plus magnetite (if present). For the original samples LimSt and

**Table 3**
Comparison of SEM-MLA and XRD data of the four laterite samples as well as of selected bioleached residues T1 of the experiments with *At. thiooxidans*.

| | MLA in area% | | XRD in wt% | | MLA in area% | | XRD in wt% | | MLA in area% | | XRD in wt% | | MLA in area% | | XRD in wt% | |
|---|---|---|---|---|---|---|---|---|---|---|---|---|---|---|---|---|
| Mineral | LimSt | LimSt T1 | LimSt | LimSt T1 | BaSt | BaSt T1 | BaSt | BaSt T1 | BaC | BaC T1 | BaC | BaC T1 | 1P5 | 1P5 T1 | 1P5 | 1P5 T1 |
| silica | 6.3 | 7.7 | 7 | 5 | 8.3 | 13.9 | 12 | 9 | 2.0 | 1.8 | 3 | 2 | 0.0 | 0.0 | | |
| Al-bearing silicates | 10.0 | 12.3 | 15 | 15 | 51.8 | 65.9 | 13 | 12 | 28.0 | 29.7 | 8 | 6 | 4.3 | 2.4 | 1 | 2 |
| Mg silicates | 0.9 | 0.6 | 4 | 2 | 16.7 | 0.7 | 14 | 11 | 0.5 | 0.4 | 6 | 13 | | | | |
| Fe-oxides/ hydroxides | 59.3 | 70.7 | 64 | 62 | 13.6 | 13.8 | 54 | 55 | 52.6 | 63.6 | 77 | 76 | 91.3 | 95.9 | 94 | 93 |
| spinel | 9.6 | 5.7 | 6 | 6 | 2.8 | 0.8 | 4 | 3 | 3.5 | 1.7 | 2 | 1 | 3.2 | 1.0 | 5 | 1 |
| Mn phases | 12.1 | 0.1 | | | 5.5 | 0.7 | | | 12.7 | 1.5 | | | 1.1 | | | |
| primary silicates | 0.2 | 0.3 | | | 0.7 | 0.4 | | | 0.3 | 0.2 | | | | | | |
| sulfur | | 0.6 | | 3 | | 1.2 | | 8 | | 0.1 | | | | 0.6 | | 3 |
| others | 1.7 | 2.2 | 3 | 6 | 0.5 | 2.8 | 2 | 1 | 0.5 | 1.1 | 4 | 2 | 0.1 | 0.2 | | |
| Total | 100 | 100 | 99 | 99 | 100 | 100 | 99 | 99 | 100 | 100 | 100 | 100 | 100 | 100 | 100 | 99 |

1P5 the SEM-MLA results fit well to the XRD data (Table 3). For the original samples BaSt and BaC the SEM-MLA results for iron oxide/hydroxides are lower compared to the XRD data, but phases grouped as Al-silicates are identified in significant amounts (52 % and 28 %) by SEM-MLA in these two samples. Very fine-grained agglomerated mixtures of various Al-bearing silicates (for example phyllosilicates) and iron oxide/hydroxides cannot be correctly separated and identified by SEM-MLA due to the excitation volume (about 5 μm in vertical and about 3 μm in horizontal dimension) of the electron beam. The fine-grained mixtures result in a combined signal in SEM-EDX and a subsequent classification of these areas as Al-bearing silicates.

Spinel mineral phases listed in Table 3 comprise spinel group minerals like chromite and magnetite for XRD data (because cubic spinel group minerals cannot be discriminated by XRD) and Cr-rich spinel for the SEM-MLA data. Therefore, chromite present in the samples was identified as magnetite by XRD.

The contents of silica phases (mostly as quartz) identified by SEM-MLA and XRD correspond well in all four original samples. Mg-bearing Al-free phyllosilicates (like serpentine and talc) were detected in significant amounts (17 %) by SEM-MLA in the original sample BaSt. These phases were detected by XRD in this sample as well (14 %). However, the quantification of these phases in laterite samples by XRD for mineral portions in the range of 10 % and below is hampered by the low degree of structural order of the phyllosilicates as well as the low crystallinity of iron oxides/hydroxides. Both effects lead to strong peak broadening, in case of structural disorder even asymmetry. In addition, the tendency to show preferred orientation of platy crystallites as well as the possible presence of amorphous components make the quantification even more uncertain. This is indicated by the observation that the talc portion given by XRD in sample BaC increased significantly from 6 % to 13 % after bioleaching, which is not plausible. Another indication for these uncertainties is that the TOF data report a MgO concentration of 0.7 % for the bioleached BaC sample, which is not compatible with a talc portion of 13 % ([MgO] = 4.1 %) obtained by XRD.

Mn phases were detected by SEM-MLA in the original samples BaSt (6 %), BaC (13 %), LimSt (12 %), and 1P5 (1 %). These phases were not detected by XRD, probably due to low degree of crystallinity of these minerals.

### 3.4.2. *Changes in mineralogy induced by bioleaching and mineralogy-based mass balances for Co and Ni in the bioleaching process*

The iron oxide/hydroxide phases goethite and hematite identified by XRD were not substantially dissolved by bioleaching. This is indicated by the fact that their portions do not differ substantially between the original samples and their bioleached residues (Table 3). This is confirmed by SEM-MLA data as the Fe-oxide/hydroxide phases are present in comparable amounts in the original and bioleached aliquots as well. XRD and SEM-MLA data show that quartz and Al-bearing silicates like chlorite were not dissolved in substantial portions by bioleaching. However, serpentine (SEM-MLA and XRD data) and Mn phases (SEM-MLA data) were no longer present in the bioleached aliquots and could be regarded as dissolved by bioleaching. In the light of the observed changes in mineralogy – e.g., Fe-oxide/hydroxide phases were not dissolved but serpentine and Mn phases were dissolved by bioleaching – Co and Ni amounts within these phases were estimated and compared to the results of bioleaching.

The portion of the Fe-oxide/hydroxide phases obtained by different mineralogical methods are given in Table 4. For the mass balance calculations, the XRD data were used, because as mentioned above the SEM-MLA data seem to underestimate these portions. Differential scanning calorimetry (DSC) or thermogravimetry (TG) is based on the mass loss upon heating and therefore primarily accounts for the goethite portions (Houben and Kaufhold, 2011). Goethite is the most important Fe-oxide/hydroxide in the samples, but Fe-oxides, which do not release water upon heating, are not included in the TG data. Results of the DSC analysis with a detailed description are given in Fig. S24 in the supplementary material. The order of the samples based on XRD and TG data is consistent with the order of the samples based on the $Fe_2O_3$ content from bulk XRF analysis.

**Table 4**
Portion of the Fe-oxide/hydroxide phases obtained by different mineralogical methods.

| Sample | XRD, mass% | SEM-MLA, area% | TG, mass% |
|---|---|---|---|
| BaSt | 54 | 14 | 32 |
| BaC | 77 | 53 | 57 |
| LimSt | 64 | 59 | 54 |
| 1P5 | 94 | 91 | 76 |

The Co and Ni contents of the Fe-oxide/hydroxide phases were estimated from the TOF data. Huge parts of the samples are very fine grained (<6 μm, see Fig. S2). A square-shaped TOF laser spot of 10*10 μm sometimes ablates different phases and results in a mixed analysis of different phases. In order to minimize this effect, areas with Fe concentrations of [Fe] > 55 % were selected from the TOF maps to obtain the Co and Ni concentrations of the Fe-oxide/hydroxide phases, as these areas were supposed to have only minor contributions of non-Fe-oxide/hydroxide phases. The mean values from all pixels with [Fe] > 55 % were calculated and used as the Co and Ni concentrations of the Fe-oxide/hydroxide phases.

The portion of serpentine (Al-free Mg silicates) was taken from the SEM-MLA data. Fig. 5 gives the Mg distribution for sample BaSt (TOF data) and the SEM-MLA map of the same area. The areas of high Mg concentrations (dark red areas) correspond well with the green areas on the SEM-MLA map indicating Al-free Mg silicates (serpentine). If the boundary conditions [Mg] > 20% and [Al] < 3 % (target: Mg-bearing Al-free phyllosilicates) are applied on the TOF data these areas can be aggregated and correspond well to the serpentine (Al-free Mg silicates) areas from the SEM-MLA map. The mean composition of these areas can be extracted from the TOF data: $SiO_2$ = 39.5 %, $Al_2O_3$ = 1.1 %, MgO = 40.5 %, $Fe_2O_3$ = 14.9 %, MnO = 0.1 %, Co = 440 mg/kg, and Ni = 25411 mg/kg. This composition is close to the ideal composition of serpentine ($SiO_2$ = 43.4 %, MgO = 43.6 %, $H_2O$ = 13 %). Areas with [Mg] > 20 % and [Al] < 3 % were not detectable any more in the bioleached BaSt sample, which indicates that this phase was dissolved by bioleaching (Fig. 5).

The portion of the Mn-bearing oxide phase and its Co and Ni concentrations could be obtained from TOF data. The portion of this phase was estimated from the TOF data because (i) XRD was not providing data for this phase and (ii) the particle size of the Mn-bearing oxide phase seemed to be larger (also visible on SEM-MLA maps) compared to the Fe-oxide/hydroxide phases and thus the probability that the TOF data included huge portions of mixed analysis seemed to be lower. Portions for these Mn phases from SEM-MLA data are also given in Table 3. Compositions obtained from TOF data for the four original and bioleached samples and areas defined by threshold values within these samples are given in Table S2.

Fig. 6 presents Co and Mn distributions of sample LimSt. High Co concentrations (dark red) correlate well with high Mn concentrations (dark red). These areas of high Co and Mn concentrations were not detectable any more in the bioleaching residue of the sample (data not shown). This was also confirmed by SEM-MLA as the Mn phases almost disappeared after bioleaching (Table 3). This indicates that the bioleaching process dissolved this phase. Areas of elevated Co and Mn concentrations in the original sample could be grouped together if a threshold value of [Mn] > 4% was applied (see Fig. 6). The mean composition of this group could be extracted from the TOF data: $SiO_2$ = 6.3 %, $Al_2O_3$ = 8.1 %, MgO = 1.2 %, $Fe_2O_3$ = 46.1 %, MnO = 26.9 %, Co = 5.4 %, and Ni = 6.0 %. According to TOF data the portion of this phase in sample LimSt was 4.2 %.

The portions of total Co and Ni appearing in different phases $P_E^m$ of the original samples can be estimated by using (i) the above given data

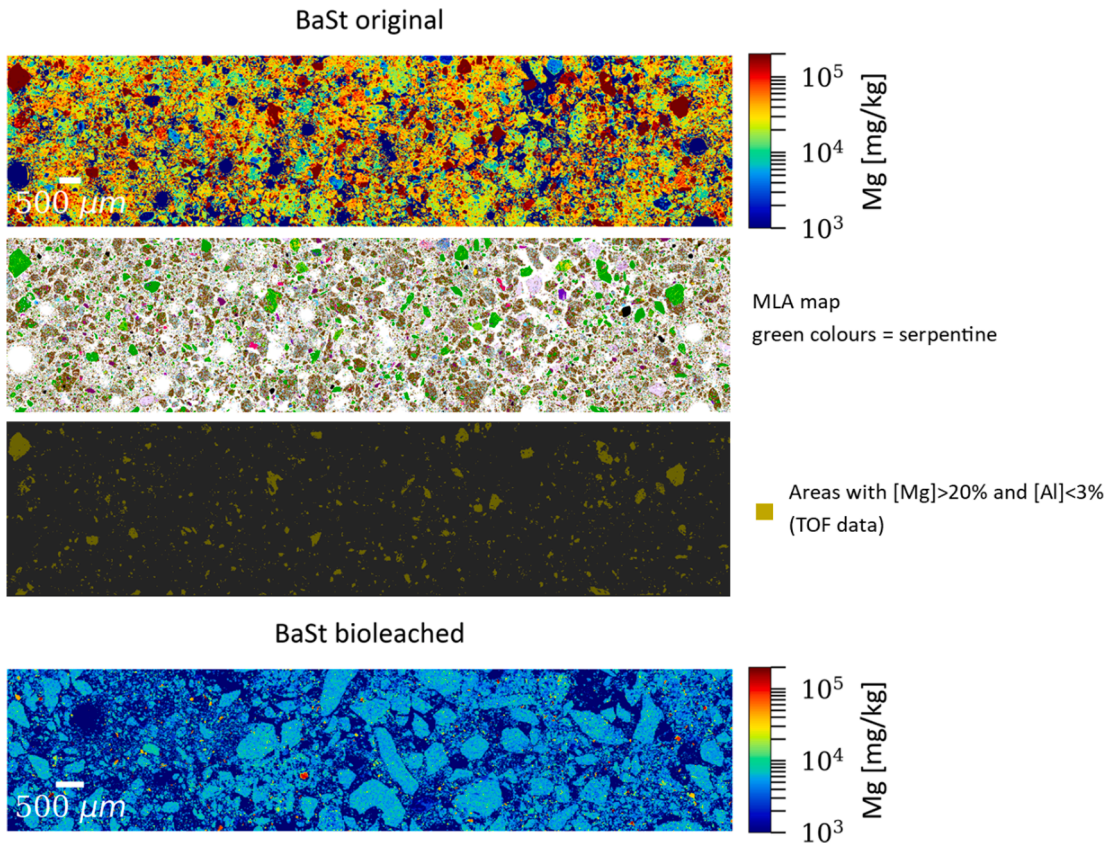


**Fig. 5.** Mg distribution in the original sample BaSt and the bioleaching residue (TOF data) and the SEM-MLA map of the same area of the original sample.

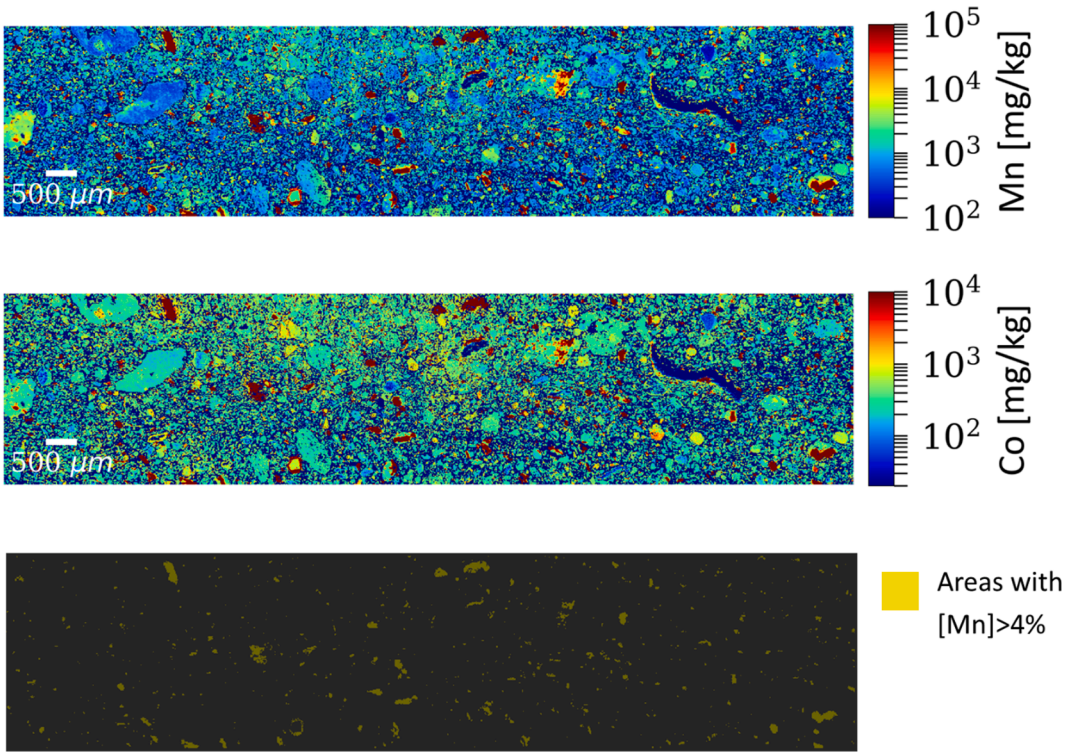


**Fig. 6.** Co and Mn distributions in the original sample LimSt (TOF data).

sources for the portions of the phases Fe-oxide/hydroxide, serpentine, and Mn phases in the original samples, (ii) the TOF data for the Co and Ni contents of these phases, and (iii) the XRF data for bulk concentrations of the samples:

$$P_E^m = \frac{P_m{}^* c_E^m}{c_E^b}$$

where $P_E^m$ gives the portion of the element E in the phase m, $P_m$ gives the portion of the phase m in the sample, $c_E^m$ gives the concentration of the element E in phase m, and $c_E^b$ gives the bulk concentration of the element E in the sample.

Under the hypothesis that Fe-oxide/hydroxides were not bioleached, and serpentine and the Mn phases were completely dissolved releasing their Co and Ni into solution, the estimated portions could be compared with the bioleaching results (Table 5). For Co and Ni, the sum of the contents sitting in the serpentine and the Mn phases roughly corresponded to the content obtained from bioleaching in all samples. The bioleached portions and the portions sitting in the not dissolved Fe-oxide/hydroxides sum up to almost all the Co and Ni in all samples. Thus, the bioleached Co and Ni largely originated from serpentine and the Mn phases. An increase in the Co and Ni yield by bioleaching could only be achieved if the Fe-oxide/hydroxide phase is dissolved as well.

### 3.5. Impact of mineralogy on bioleaching of laterites

A different leaching behavior of limonitic laterites, even ones coming from the same ore deposit, is obviously a consequence of their different mineralogical composition. The sample designated as 1P5 was constituted almost exclusively of Fe(III)-containing minerals (goethite, hematite and magnetite). Leaching degrees of nickel and cobalt were negligible even after leaching with high concentrations of sulfuric acid and hydrochloric acid. The DSC data shown in Fig. S24 indicate a higher crystallinity of the goethite in sample 1P5 than for the other ones. Goethite and hematite are very difficult to dissolve, an efficient leaching of these minerals requires elevated pressure and temperatures in a high-pressure acid leaching process (Whittington and Muir, 2000). The highest leaching degrees of nickel were achieved after reductive bioleaching of the BaSt sample, which contained the lowest amount of iron and the highest amount of serpentine minerals among all four samples of this study. The content of iron-rich phases remained equal or even increased in all bioleaching residues, meaning that it was not possible to achieve satisfactory dissolution of Fe-rich mineral phases. But this approach was efficient in leaching of Co-containing mineral phases (Mn phases) and Mg-rich phases, such as minerals from the serpentine group. Serpentine group minerals dissolve after proton attack producing poorly crystalline silica residues much depleted in Mg and Ni (Hunter et al., 2013). The findings of our study do not support the described reductive bioleaching of goethite by *At. ferrooxidans* (e.g. Hallberg et al., 2011; Johnson et al., 2013). These studies could demonstrate Ni and Co bioleaching from limonitic laterites, however the presented mineralogical data were not quantitative and could not resolve the dissolution of goethite which has now to be considered as a false interpretation of the data.

**Table 5**
Portions of total Co and Ni [%] estimated for different phases in untreated samples and bioleached portions [%].

| Sample | Element | Co and Ni carried by phase | | | Bioleached |
|---|---|---|---|---|---|
| | | Fe-oxide/ hydroxide | Serpentine | Mn phases | |
| BaC | Co | 25 | 0 | 53 | 79 |
| | Ni | 73 | 0 | 11 | 20 |
| BaSt | Co | 18 | 6 | 53 | 77 |
| | Ni | 62 | 32 | 9 | 48 |
| LimSt | Co | 14 | 0 | 85 | 86 |
| | Ni | 63 | 0 | 17 | 23 |
| 1P5 | Co | 90 | 0 | 0 | 3 |
| | Ni | 86 | 0 | 0 | 1 |

The mineralogical and geochemical results or our study show that the samples LimSt and BaC had similar properties. The majority of bioleachable Ni and Co was released by reductive dissolution of Mn phases. Sample BaSt contained Mn phases and additional serpentine. Here the dissolution of serpentine during bioleaching released the majority of bioleached Ni. Sample 1P5 did not contain any serpentine or Mn phases, which resulted in very low amounts of released Co and Ni in bioleaching. This sample 1P5 was taken from one locality of the limonitic horizon in the open pit and consisted almost entirely of iron hydroxide/oxide. Sample BaC represented a bulk sample mixed from channel samples taken at three different localities of the limonitic horizon. However, the composition of the laterite deposit was not homogenous laterally and vertically, which is also indicated by a composition of BaC that is less dominated by iron hydroxide/oxide compared to the almost pure limonite represented by sample 1P5. The two samples LimSt and BaSt represented samples from two different stockpiles. Sample LimSt was taken from the surface of a stockpile and due to its similar properties to sample BaC, sample LimSt looked like a stockpiled version of sample BaC material. The stockpile sample BaSt originated from a 16 m deep borehole and contained serpentine. As serpentine is a typical mineral found in saprolites, sample BaSt did not contain only limonitic material but also saprolitic portions. This is not surprising having the length of the borehole in mind from which this sample was taken and the fact that other materials like overburden or saprolite were also dumped together with limonite.

The results presented in this paper are in accordance with previously published results on aerobic and anaerobic reductive bioleaching of the limonitic laterite overburden of a Cuban laterite mine (Marrero et al., 2017). The authors reported a leaching degree of cobalt in bioreactors inoculated with *At. thiooxidans* of 85 % and in bioreactors inoculated with *At. ferrooxidans* of 78 %. The leaching degree of nickel in both bioreactors was low and reached 16 %. Mineralogical analysis of the leaching residues showed that the share of goethite in the leaching residue increased in comparison to the original sample, indicating that this mineral was not dissolved during the bioleaching experiment (Marrero et al., 2017). Santos et al. (2020) reported relatively low cobalt extractions during anaerobic reductive bioleaching of three laterite samples from Greece (39 %, 40 % and 49 %), but a relatively high extraction of nickel from two of these samples (73 % and 68 %). The sample from which 73 % of nickel was extracted contained the highest amount of the serpentine mineral and the content of this mineral was significantly reduced in the leaching residue. Serpentine, chlorite, talc and smectite minerals were present in all samples. Santos et al. reported lowest nickel (37 %) and iron (2 %) extractions from the sample which contained the highest amount of goethite and total iron. Smith et al. (2017) reported a high leaching degree of cobalt from three limonitic laterite samples (>99 %, 88.5 % and 90 %) using a bacterial consortium under anaerobic conditions, but nickel extraction differed significantly between these samples (>70 %, 50 % and 40 %). Nickel and cobalt extractions during reductive bioleaching of the limonitic laterites reported in this and cited papers differ largely depending on the ore mineralogy. Extraction of Ni from laterites decreases with increasing content of goethite, but in some lateritic deposits goethite might be unusually reactive and therefore rapidly dissolved by acid (Watling et al., 2011). Reductive bioleaching needs some improvements in order to become a viable technology applicable for treatment of goethite-rich lateritic ore from the Barro Alto mine as well as other mines.

## 4. Conclusions

This study has shown that the efficiency of bioleaching and chemical leaching of limonitic laterite ores strongly depends on their mineralogy. Even samples from the same ore deposit showed substantial differences with consequences for ore processing. Cobalt extraction based on

reductive bioleaching could successfully be demonstrated while Ni extraction via bioleaching requires further improvement. It can be concluded that limonitic laterites with lower iron content and higher content of Mg-rich mineral phases, such as serpentine, perform better during reductive bioleaching. For the first time, quantitative mineralogical analyses of laterite ores in comparison to bioleaching residues allowed for describing which mineral phases with particular Co and Ni contents were dissolved in the leaching process as a tool for ore processing optimization.

*CRediT authorship contribution statement*

**Srdjan Stanković:** Conceptualization, writing original draft, bioleaching experiments. **Mirko Martin:** Conceptualization, samples preparation, chemical leaching experiments, funding acquisition. **Simon Goldmann:** Sampling, SEM-MLA, data validation, writing and editing. **Hans-Eike Gäbler:** LA-ICP-TOFMS, data validation, writing, review and editing. **Kristian Ufer:** XRD, DSC, samples physical properties, writing. **Frank Haubrich:** Conceptualization, samples preparation, chemical leaching experiments, funding acquisition. **Vivian Fernandes Moutinho:** Conceptualization, samples preparation, SEM-EDX. **Ellen Cristine Giese:** Conceptualization, samples preparation, SEM-EDX. **Reiner Neumann:** Conceptualization, samples preparation, SEM-EDX. **José Luciano Stropper:** Conceptualization, sampling, project administration. **Jens Stummeyer:** ICP-OES, XRF, data validation. **Stephan Kaufhold:** XRD, DSC, samples physical properties, writing. **Reiner Dohrmann:** XRD, DSC, samples physical properties, writing. **Anne Oxley:** Conceptualization, sampling. **Herwig Marbler:** Conceptualization, sampling, funding acquisition, project administration. **Axel Schippers:** Conceptualization, writing, review and editing, funding acquisition, project administration.

## Declaration of Competing Interest

The authors declare that they have no known competing financial interests or personal relationships that could have appeared to influence the work reported in this paper.

## Acknowledgements

We thank the company Anglo American in Brazil for providing samples. The joint research was carried out based on the BioCobalt agreement and the BioProLat research proposal. It was financially supported by the German Mineral Resources Agency (DERA) within BGR as well as by the German Federal Ministry of Education and Research (BMBF), CLIENT II project BioProLat, FKZ 033R271A.

## Appendix A. Supplementary material

Supplementary data to this article can be found online at https://doi.org/10.1016/j.mineng.2022.107604.

## References

Bergmann, J., Friedel, P., Kleeberg, R., 1998. BGMN – a new fundamental parameters based Rietveld program for laboratory X-ray sources, its use in quantitative analysis and structure investigations. CPD Newsl. (Commission of Powder Diffraction, International Union of Crystallography) 20, 5–8.

Brand, N.W., Butt, C.R.M., Elias, M., 1998. Nickel laterites: classification and features, AGSO. J. Austral. Geol. Geophys. 17, 81–88.

Bridge, T.A.M., Johnson, D.B., 2000. Reductive dissolution of ferric iron minerals by *Acidiphilium* SJH. Geomicrobiol. J. 17, 193–206.

Döbelin, N., Kleeberg, R., 2015. Profex: a graphical user interface for the Rietveld refinement program BGMN. J. Appl. Crystallogr. 48 (5), 1573–1580.

du Plessis, C.A., Slabbert, W., Hallberg, K.B., Johnson, D.B., 2011. Ferredox: A biohydrometallurgical processing concept for limonitic nickel laterites. Hydrometallurgy 109, 221–229.

Fandrich, R., Gu, Y., Burrows, D., Moeller, K., 2007. Modern SEM-based mineral liberation analysis. Int. J. Miner. Process. 84 (1-4), 310–320.

Hallberg, K.B., Grail, B.M., Plessis, C.A.d., Johnson, D.B., 2011. Reductive dissolution of ferric iron minerals: A new approach for bio-processing nickel laterites. Min. Eng. 24 (7), 620–624.

Handler, R.M., Beard, B.L., Johnson, C.M., Scherer, M.M., 2009. Atom exchange between aqueous Fe(II) and goethite: an Fe isotope tracer study. Environ. Sci. Technol. 43 (4), 1102–1107.

Hedrich, S., Guézennec, A.G., Charron, M., Schippers, A., Joulian, C., 2016. Quantitative monitoring of microbial species during bioleaching of copper concentrate. Front. Microbiol. 7, 2044.

Houben, G., Kaufhold, S., 2011. Multi-method characterization of the ferrihydrite to goethite transformation. Clay Minerals 46 (3), 387–395.

Hunter, H.M.A., Herrington, R.J., Oxley, E.A., 2013. Examining Ni-laterite leach mineralogy and chemistry – a holistic multi scale approach. Min. Eng. 54, 100–109.

Johnson, D.B., du Plessis, C.A., 2015. Biomining in reverse gear: Using bacteria to extract metals from oxidised ores. Min. Eng. 75, 2–5.

Johnson, D., Grail, B., Hallberg, K., 2013. A new direction for biomining: Extraction of metals by reductive dissolution of oxidized ores. Minerals 3 (1), 49–58.

Kaufhold, S., Dohrmann, R., Klinkenberg, M., Siegesmund, S., Ufer, K., 2010. N2-BET specific surface area of bentonites. J. Colloid Interface Sci. 349 (1), 275–282.

Komnitsas, K., Petrakis, E., Bartzas, G., Karmali, V., 2019. Column leaching of low-grade saprolitic laterites and valorization of leaching residues. Sci. Tot. Environ. 665, 347–357.

Li, G., Rao, M., Jiang, T., Huang, Q., Peng, Z., 2011. Leaching of limonitic laterite ore by acidic thiosulfate solution. Min. Eng. 24 (8), 859–863.

Lovley, D.R., Phillips, E.J.P., 1987. Rapid assay for microbially reducible ferric iron in aquatic sediments. Appl. Environ. Microbiol. 53 (7), 1536–1540.

Luo, J., Li, G., Rao, M., Peng, Z., Zhang, Y., Jiang, T., 2015. Atmospheric leaching characteristics of nickel and iron in limonitic laterite with sulfuric acid in the presence of sodium sulfite. Min. Eng. 78, 38–44.

McDonald, R.G., Whittington, B.I., 2008. Atmospheric acid leaching of nickel laterites review Part I. Sulfuric acid technologies. Hydrometallurgy 91 (1-4), 35–55.

Malik, L., Hedrich, S., 2022. Ferric iron reduction in extreme acidophiles. Front. Microbiol. 12, 818414.

Marrero, J., Coto, O., Schippers, A., 2020. Metal bioleaching: fundamentals and geobiotechnical application of aerobic and anaerobic acidophiles. In: Lee, N.M. (Ed.), Biotechnological Applications of Extremophilic Microorganisms. Walter de Gruyter GmbH, Berlin, Munich, Boston, pp. 261–287.

Marrero, J., Coto, O., Goldmann, S., Graupner, T., Schippers, A., 2015. Recovery of nickel and cobalt from laterite tailings by reductive dissolution under aerobic conditions using *Acidithiobacillus* species. Environ. Sci. Technol. 49 (11), 6674–6682.

Marrero, J., Coto, O., Schippers, A., 2017. Anaerobic and aerobic reductive dissolutions of iron-rich nickel laterite overburden by *Acidithiobacillus*. Hydrometallurgy 168, 49–55.

Müller, H.-W., Dohrmann, R., Klosa, D., Rehder, S., Eckelmann, W., 2009. Comparison of two procedures for particle size analysis: KÖHN-pipette and X-ray granulometry. J. Plant Nutr. Soil Sci. 172 (2), 172–179.

Santos, A., Schippers, A., 2022. Reductive mineral bioprocessing. In: Bryan, C.G., Johnson, D.B., Roberto, F.F., Schlömann, M. (Eds.), Biomining, Springer, in press.

Santos, A.L., Dybowska, A., Schofield, P.F., Herrington, R.J., Johnson, D.B., 2020. Sulfur-enhanced bioprocessing of cobalt bearing materials for base metal recovery. Hydrometallurgy 195, 105396.

Schippers, A., 2007. Microorganisms involved in bioleaching and nucleic acid-based molecular methods for their identification and quantification. In: Microbial Processing of Metal Sulfides. E. R. Donati and W. Sand (eds.). Springer, 3–33. ISBN: 978-1-4020-5588.

Schwertmann, U., 1991. Solubility and dissolution of iron oxides. Plant Soil 130 (1-2), 1–25.

Senanayake, G., Childs, J., Akerstrom, B.D., Pugave, D., 2011. Reductive acid leaching of laterite and metal oxides – A review with new data for Fe(Ni, Co)OOH and limonitic ores. Hydrometallurgy 110, 13–32.

Smith, S.L., Grail, B.M., Johnson, D.B., 2017. Reductive bioprocessing of cobalt bearing limonitic laterites. Min. Eng. 106, 86–90.

Stanković, S., Stopić, S., Sokić, M., Marković, B., Friedrich, B., 2020. Review of the past, present and future of the hydrometallurgical production of nickel and cobalt from lateritic ores. Metall. Mater. Eng. 26 (2), 199–208.

Wakeman, K., Auvinen, H., Johnson, D.B., 2008. Microbiological and geochemical dynamics in simulated-heap leaching of a polymetallic sulfide ore. Biotechnol. Bioeng. 101 (4), 739–750.

Watling, H.R., Elliot, A.D., Fletcher, H.M., Robinson, D.J., Sully, D.M., 2011. Ore mineralogy of nickel laterites: control on process characteristics under simulated heap-leach conditions. Austr. J. Earth Sci. 58, 725–744.

*Whittington, B.I., Muir*, D., 2000. Pressure acid leaching of nickel laterites: a review. Min. Proc. Extr. Metall. Rev. 21 (6), 527–599.

Zhang, R., Hedrich, S., Römer, F., Goldmann, D., Schippers, A., 2020. Bioleaching of cobalt from Cu/Co-rich sulfidic mine tailings from the polymetallic Rammelsberg mine, Germany. Hydrometallurgy 197, 105443. https://doi.org/10.1016/j.hydromet.2020.105443.